Electric Field-Induced Giant Strain and Photoluminescence-Enhancement Effect in Rare-Earth Modified Lead-Free Piezoelectric Ceramics

Qirong Yao,[†] Feifei Wang,*,[†,‡] Feng Xu,[§] Chung Ming Leung,[∥] Tao Wang,[†] Yanxue Tang,[†] Xiang Ye,[†] Yiqun Xie,[†] Dazhi Sun,[†] and Wangzhou Shi[†]

[†]Key Laboratory of Optoelectronic Material and Device, Department of Physics, Shanghai Normal University, Shanghai 200234, China

[‡]Centre for Advanced Materials Technology (CAMT), School of Aerospace, Mechanical and Mechatronic Engineering, The University of Sydney, Sydney, NSW 2006, Australia

[§]School of Aeronautics, Northwestern Polytechnical University, Xi'an, Shanxi 710072, China

[∥]Department of Electrical Engineering, The Hong Kong Polytechnic University, Hung Hom, Kowloon, Hong Kong

Ⓢ Supporting Information

ABSTRACT: In this work, an electric field-induced giant strain response and excellent photoluminescence-enhancement effect was obtained in a rare-earth ion modified lead-free piezoelectric system. Pr^{3+}-modified $0.93(Bi_{0.5}Na_{0.5})TiO_3$-$0.07BaTiO_3$ ceramics were designed and fabricated by a conventional fabrication process. The ferroelectric, dielectric, piezoelectric, and photoluminescence performances were systematically studied, and a schematic phase diagram was constructed. It was found the Pr^{3+} substitution induced a transition from ferroelectric a long-range order structure to a relaxor pseudocubic phase with short-range coherence structure. Around a critical composition of 0.8 mol % Pr^{3+}, a giant reversible strain of ~0.43% with a normalized strain S_{max}/E_{max} of up to 770 pm/V was obtained at ~5 kV/mm. Furthermore, the *in situ* electric field enhanced the photoluminescence intensity by ~40% in the proposed system. These findings have great potential for actuator and multifunctional device applications, which may also open up a range of new applications.

KEYWORDS: *piezoelectric, photoluminescence, ferroelectric polarization, lead-free, strain*
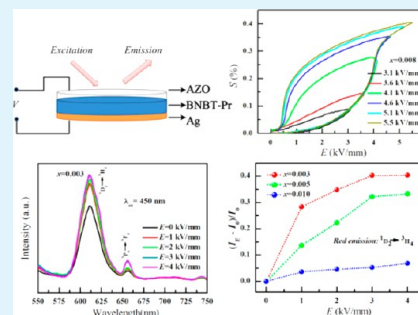
1. INTRODUCTION

Recently, smart materials have stimulated great scientific and technological interest because of their outstanding coupling functions among the electric, magnetic, mechanical, caloric, and optical properties. Various two-parameter coupling effects have been observed and extensively studied in the scientific community such as electro-mechanical,[1] electro-magnetic,[2] electro-optical,[3] magneto-optical,[4] and electro-caloric coupling effects.[5] With the development of the functional material and device, it is desirable to develop new coupling effects with multiple functions in single-phase materials. As previously reported, multiple simultaneous electro-mechano-optical conversions were achieved in a Pr-doped system, which combined the piezoelectric and electroluminescent effect.[6] However, to the best of our knowledge, multiple-function coupling in a single-phase system was quite limited.

Because of the significant applications in sensors, actuators, and display devices, two important smart systems, piezoelectric and photoluminescence (PL) materials, have attracted extensive attention during the past few decades. For the piezoelectric material, until now, the dominant one is still the lead zirconate titanate (PZT) ceramic because of its outstanding electro-

mechanical properties. Nevertheless, the lead is toxic, and developing lead-free substitutes that can compete with PZT has received great interest recently.[7] Even though some lead-free materials with both improved piezoelectric performance and strain response were obtained, the global electrical properties of the lead-free systems are still inferior compared to those of PZT.[8] Therefore, it is quite important to further enhance the piezoelectric response for device applications. For PL materials, modulation and enhancement of the PL effect is now being extensively studied, because it is important for various optical device applications.[9−12] Traditional modulation was mainly based on the chemical approach that was generally irreversible, and the modulation was an *ex situ* way. It is quite necessary to develop other *in situ* turning methods for PL modulation and enhancement.[9]

In this work, a single-phase multifunctional system, namely Pr-modified $(Bi_{0.5}Na_{0.5})TiO_3$-$BaTiO_3$, that could lead to electro-mechano-optical conversions through a combination of the
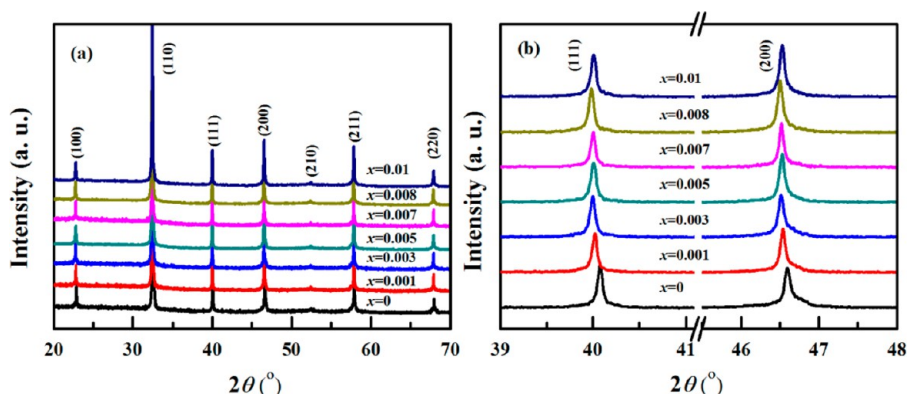
Figure 1. Room-temperature XRD results for the BNBT-xPr system in the ranges of (a) 20−70° and (b) 39−48°.

piezoelectric and PL effects was prepared. The coupling behavior between the two effects was carefully studied. It was found that both the ferroelectric and piezoelectric performances were substantially improved and the normalized strain S_{max}/E_{max} could reach 770 pm/V. Furthermore, an enhancement of the PL intensity by ~40% was achieved because of the local symmetry variation induced by the ferroelectric polarization. The corresponding mechanisms for the giant strain response and piezoelectric/photoluminescence coupling effects are discussed.

2. EXPERIMENTAL DETAILS

2.1. Synthesis of Materials. During the experiment, 0.93-$(Bi_{0.5}Na_{0.5})TiO_3$-$0.07BaTiO_3$ was chosen as the starting composition because of its excellent piezoelectric and electromechanical performances.[13,14] The proposed system $0.93(Bi_{0.5}Na_{0.5})TiO_3$-$0.07BaTiO_3$-$x$Pr (BNBT-$x$Pr, where x = 0, 0.001, 0.003, 0.005, 0.007, 0.008, or 0.010) was prepared through the traditional solid state reaction method. The starting materials Bi_2O_3 (99.0%), $BaCO_3$ (99.0%), Na_2CO_3 (99.8%), TiO_2 (98.0%), and Pr_6O_{11} (99.9%) were utilized, and the details of the fabrication of the BNBT-xPr ceramics have been described previously.[15]

2.2. Characterization. The phase structures were characterized using XRD (D8 Focus, Bruker AXS, Karlsruhe, Germany). The microstructure and element mapping were measured by a field emission scanning electron microscope (FESEM, S-4800, Hitachi, Tokyo, Japan). The ferroelectric domain structure was measured by piezoresponse force microscopy (PFM, MFP-3D, Asylum Research). The temperature and frequency dependence of the dielectric constant and loss were recorded using an Agilent (Santa Clara, CA) HP4294A analyzer. The ferroelectric properties and strain performance were acquired using a TF2000 analyzer (Aixacct, Aachen, Germany). The composition- and field-dependent PL and PL excitation spectra were recorded using a fluorescence spectrophotometer (Cary Eclipse, Agilent) at room temperature. The Raman data were recorded using the SuperLabRam II Raman system (Dilor, France). The quasi-static piezoelectric constant d_{33} of the ceramics was measured by a Berlincourt d_{33} meter. The electromechanical coupling coefficients (k_t) were calculated from the following formula based on the IEEE standards[16]

$$k_t^2 = \frac{\pi f_r}{2f_a} \tan\left[\frac{\pi(f_a - f_r)}{2f_a}\right]$$

(2)

where f_r and f_a represent resonance and antiresonance frequencies, respectively.

3. RESULTS AND DISCUSSION

3.1. Phase Structure and Electric Field-Induced Giant Strain Response. Figure 1a illustrates the XRD results for the sintered BNBT-xPr ceramics. All the ceramics possessed pure single-phase perovskite structure. To clarify the phase structure, XRD with a 2θ in the range of 39−48° was conducted at a slow

scanning rate, and the results are shown in Figure 1b. From Figure 1b, the diffraction peaks shifted slightly to the left after the introduction of Pr^{3+}. It is known that the ionic radius of Pr^{3+} (1.18 Å) is close to those of Bi^{3+} (1.17 Å) and Na^+ (1.39 Å).[17] The XRD results indicate that the Pr^{3+} mainly entered the A-site and replaced the Bi^{3+}, resulting in the slight expansion of the lattice. It could be observed that all the composition exhibited pseudocubic or cubic phase characterized by the single (111) and (200) peaks. However, slight rhombohedral or tetragonal distortion could not be excluded. Note that weak piezoelectric constant d_{33} could still be detected for BNBT-xPr with x up to 0.01. Similar pseudocubic structure has been observed in previous lead-free solid solutions.[18−20]

To reveal the structure of the samples, Raman spectroscopy and PFM were employed here. Figure 2 shows the Raman
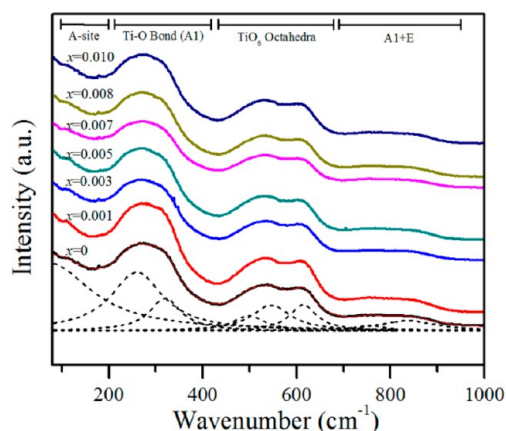
Figure 2. Raman data for BNBT-xPr ceramics at room temperature.

spectroscopy for the BNBT-xPr ceramics. Three main regions can be observed: (a) the 260 cm^{-1} mode (related to Ti−O vibrations), (b) the 450−700 cm^{-1} host modes (related to the TiO_6 octahedral vibrations), and (c) the region above 700 cm^{-1} modes [related to A_1 (longitudinal optical) and E (longitudinal optical) overlapping bands].[21] From Figure 2, two distinct splitting bands near 260 cm^{-1} could be observed for all the compositions, indicating their rhombohedral and tetragonal coexistence.[22] With the concentration x increasing, little variation in the Raman data was observed, which may be ascribed to the low concentration of the modifiers.[21]

Figure 3 shows three representative piezoresponse amplitude and phase images for BNBT, BNBT-0.008Pr, and BNBT-0.01Pr. In the piezoresponse phase images, the polarization directions of
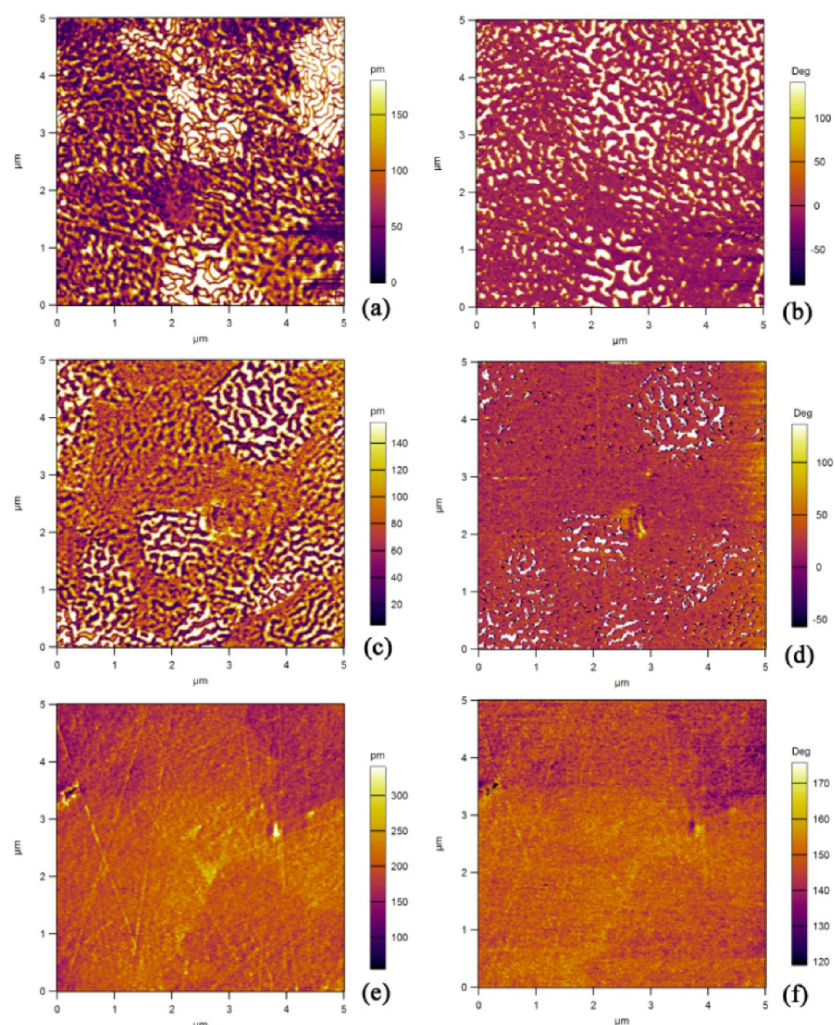
Figure 3. (a, c, and e) Piezoresponse amplitude images and (b, d, and f) piezoresponse phase images for BNBT-xPr with x values of 0, 0.008, and 0.10 in a 5 μm × 5 μm area.

the areas with dark contrast are the opposite of those with bright contrast.[23] For BNBT with a low Pr concentration, clear contrast could be observed, indicating a multidomain state (the data for BNBT are shown in panels a and b of Figure 3). With the concentration x increasing, the contrast of the piezoresponse phase image became blurred (as shown in Figure 3d for BNBT-0.008Pr) and finally disappeared (panels e and f of Figure 3 for BNBT-0.01Pr). On the basis of the description given above, the increase in the Pr concentration was found to induce a transformation of the material from typical ferroelectric structure to "non-ferroelectric" state.
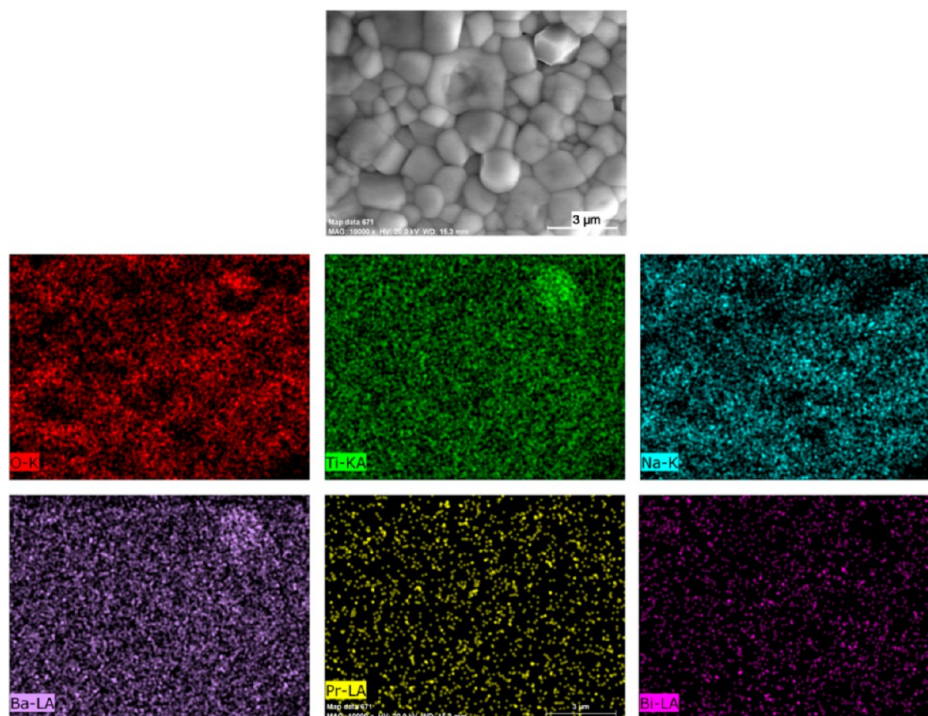
Figure 4 shows the morphology and elemental distribution of the BNBT-0.005Pr ceramic. Well-sintered, homogeneous, and dense microstructure with a grain size of ∼1–3 μm can be observed and all the elements distributed homogeneously in the system according to the energy disperse spectrum (EDS) results.

Figure 5a−c illustrates the temperature dependence of the dielectric constant ($\varepsilon_{33}^{T}/\varepsilon_0$) and loss (tan δ) for poled BNBT-xPr with three representative compositions x of 0, 0.003, and 0.008 under 100 to 10 kHz. All the curves exhibited a broad dielectric constant peak, demonstrating an obvious diffused phase transition process, which was related to the A-site multiple complexes of ions (such as Bi^{3+}, Na^{1+}, Ba^{2+}, etc.) of perovskite compounds.[24] The permittivity-maximum temperature T_m and

ferroelectric-to-relaxor transition temperature T_{F-R}[25] (determined from the loss peak) are indicated by the arrows in Figure 5a−c. Apart from T_m and T_{F-R}, another characteristic temperature, T_{DV},[15] was also manifested. From Figure 5a−c, frequency dispersion weakened obviously at room temperature in polarized BNBT-xPr ceramics with a low Pr^{3+} concentration, because of the formation of the macrodomain structure. With x increasing, T_{F-R} was shifted to a value below room temperature and the electric field could not establish long-range order, and thus, frequency dispersion could still be observed at room temperature. Furthermore, it should be noticed that after the BNBT-xPr ceramics were poled, obvious relaxor characteristics could still be observed between T_{F-R} and T_{DV}, indicating a different nature of the structure. Both T_{DV} and T_{F-R} decreased with x increasing, and the corresponding relaxor region also shifted in a lower-temperature direction. On the basis of the observation of the double hysteresis loop, some investigations proposed that the antiferroelectric phase was the dominant one for the relaxor region.[13] Actually, the BNT-based system has a quite complicated composition- and temperature-induced phase transition process, and the intrinsic nature of this relaxor region is still controversial.[26] To analyze the degree of relaxation, the following formula was used

$$\ln(1/\varepsilon - 1/\varepsilon_m) + \ln C = \gamma \ln(T - T_m) \tag{1}$$

Figure 4. Morphology and elemental distribution of the BNBT-0.005Pr ceramic.
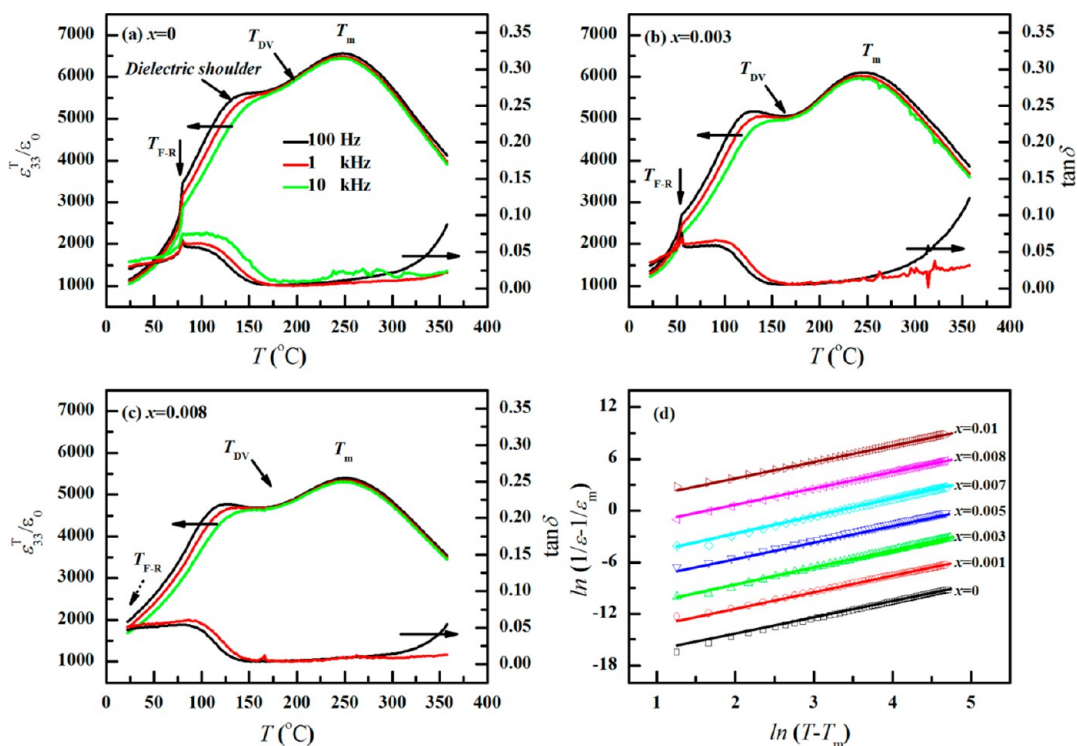

Figure 5. (a−c) Temperature-dependent dielectric constant $\varepsilon_{33}^T/\varepsilon_0$ and loss $\tan\delta$ of the poled BNBT-xPr with x values of 0, 0.003, 0.008. (d) Relations between $\ln(1/\varepsilon - 1/\varepsilon_m)$ and $\ln(T - T_m)$ for BNBT-xPr ceramics.

where C is a material-dependent constant, ε and ε_m correspond to $\varepsilon_{33}^T/\varepsilon_0$ and the maximal $\varepsilon_{33}^T/\varepsilon_0$, respectively, and γ is the degree of diffuseness.[27] On the basis of the formula given above, the γ could be determined and located between 1.79 and 1.98 as shown in Figure 5d, exhibiting relaxor characteristics.

Figure 6 shows three typical ferroelectric loops ($P-E$), polarization current curves ($I-E$), and strain curves ($S-E$) of

BNBT-xPr with x values of 0, 0.003, and 0.008. From Figure 6, it could be found that with an increase in concentration x, the $P-E$ loop developed from a typical rectangular shape to pinched loops at room temperature and the $S-E$ curves varied from typical butterfly-shaped curves to deformed ones. Similar behavior has been observed and discussed in our previous work.[15] Here the composition dependence of the ferroelectric and strain perform-
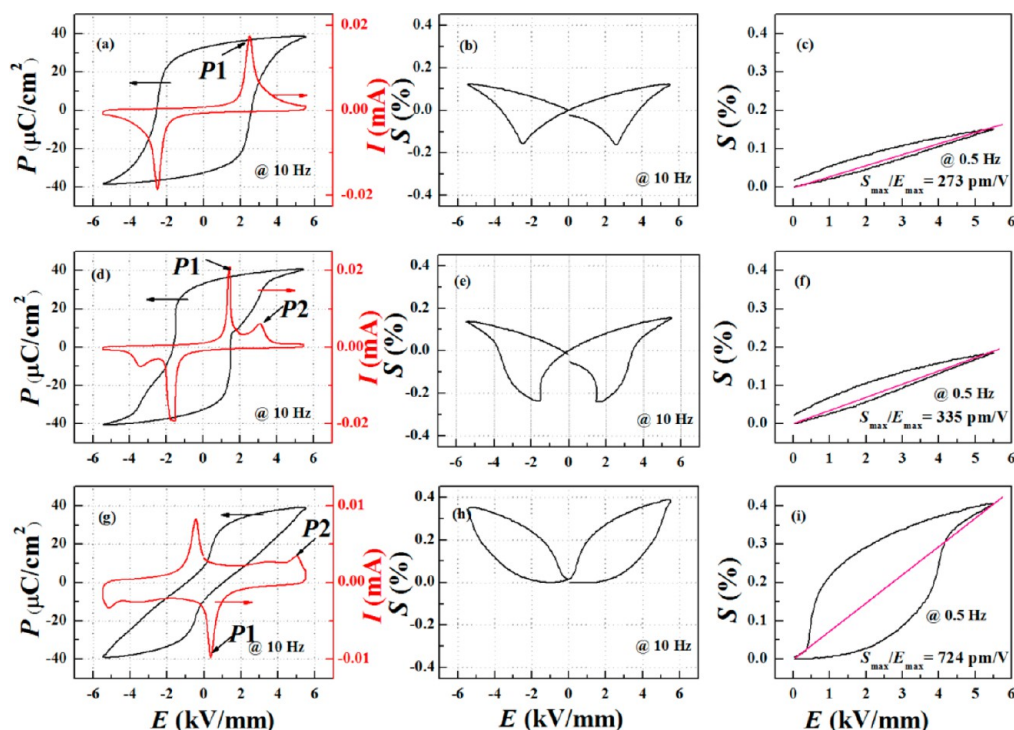
Figure 6. Ferroelectric loops ($P-E$) and polarization current curves ($I-E$) (a, d, and g), electric field-induced bipolar strain curves ($S-E$) (b, e, and h), and unipolar strain curves ($S-E$) (c, f, and i) of BNBT-xPr with x values of 0, 0.003, and 0.008.
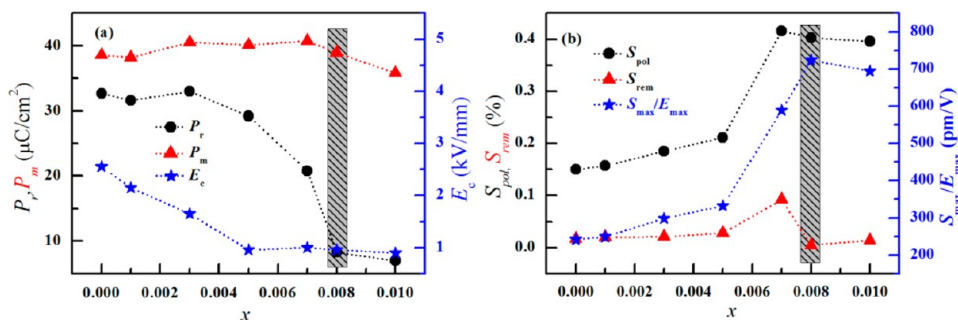
Figure 7. Composition-dependent (a) ferroelectric properties [maximal polarization (P_m), remnant polarization (P_r), and coercive field (E_c)] and (b) piezoelectric response [poling strain (S_{pol}), remnant strain (S_{rem}), and normalized strain (S_{max}/E_{max})] at room temperature.

ance was summarized in Figure 7. With the composition x increasing from 0 to 0.01, the maximal polarization P_m almost remained constant while the remnant polarization P_r displayed a sharp decrease at an x of 0.008, indicating a disruption of the ferroelectric long-range order structure. The corresponding poling strain S_{pol} (the difference value between the maximal unipolar strain and the strain under zero electric field) and remnant strain S_{rem} (the strain value when the electric field returned to zero) both first increased to a maximum and then decreased. At an x of 0.008, a giant normalized strain S_{max}/E_{max} of up to 724 pm/V was obtained.

Furthermore, the strain responses under different electric fields and frequencies were also studied here. The corresponding results for BNBT-0.008Pr are shown in Figure 8a−d. From panels a and b of Figure 8, with the field E increasing, the normalized S_{max}/E_{max} first increased and then followed a slight decrease. A maximal S_{max}/E_{max} value of 750 pm/V could be achieved at ~4.6 kV/mm and 0.5 Hz. With the frequency increasing, S_{max}/E_{max} decreased from 770 to 484 pm/V. As far as

we know, the S_{max}/E_{max} value close to 800 pm/V is the highest one reported at present for lead-free ceramics.[28]

From the characterizations and analysis presented above, a schematic phase diagram was constructed for the polarized BNBT-xPr as shown in Figure 9. The increase in the composition induced evolution of the structure from ferroelectric long-range order to relaxor (ergodic) pseudocubic, and a critical composition at an x of 0.008 was determined. In addition, the temperature dependence of the ferroelectric $P-E$ and bipolar and unipolar strain $S-E$ curves was also investigated in detail to provide an insight into the temperature-dependent behavior. The results are shown in Figures S1−S3 of the Supporting Information. It was found that in addition to the composition modification effect, the increase in temperature could also disrupt the ferroelectric long-range order above the T_{F-R}, accompanied by a large strain response. This was also similar to the composition-dependent behavior, which was observed and discussed in our previous works.[23,29]

3.2. Composition-Dependent PL Properties. Figure 10 illustrates the PL excitation and emission spectra of the
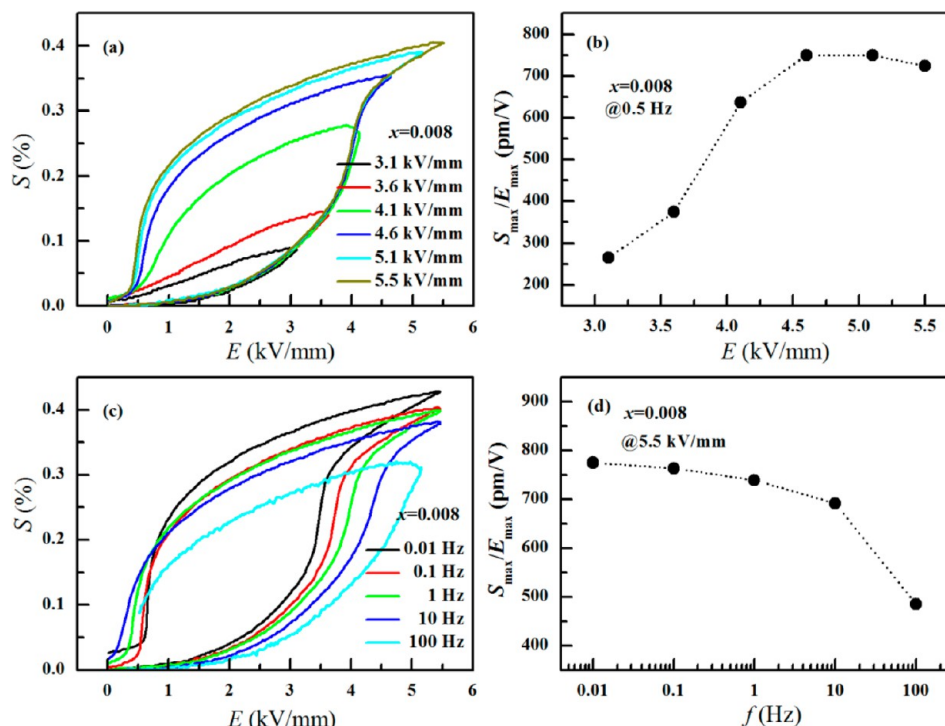
Figure 8. Unipolar strain response (a and c) and the normalized strain S_{max}/E_{max} (b and d) as a function of frequency and electric field.
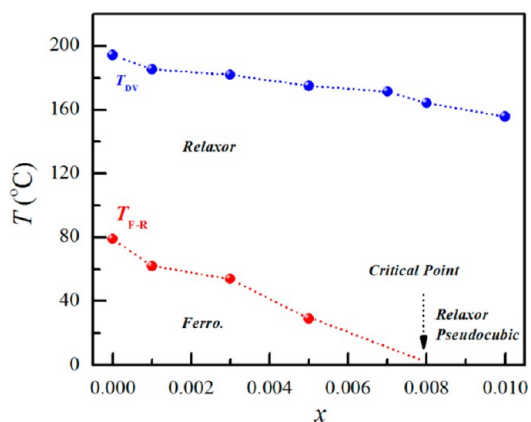

Figure 9. Schematic phase diagram for the BNBT-xPr system.

unpolarized BNBT-xPr with x values of 0.001, 0.003, 0.005, 0.007, and 0.008. The characteristic peaks exhibited no obvious shifting for any of the samples. From the excitation spectra of BNBT-xPr ceramics monitored at a λ_{em} of 612 nm as shown in

Figure 10a, three strong excitation peaks between 440 and 500 nm could be observed. The broad excitation band between 350 and 425 nm was ascribed to the $Pr^{3+}(4f) \rightarrow Ti^{4+}(3d)$ charge transition and the absorption of Bi^{3+} ions.[30−32] The excitation peaks between 440 and 500 nm originated from the 4f–4f transition from the $^3H_4$ ground state to the ^3P_J (J = 0, 1, or 2) excited state of Pr^{3+} ions. Specifically, the intensity peaks at 452, 478, and 494 nm corresponded to the $^3H_4 \rightarrow {}^3P_2$, $^3H_4 \rightarrow {}^3P_1$, and $^3H_4 \rightarrow {}^3P_0$ transitions, respectively.[33] Figure 10b illustrates the PL emission of BNBT-xPr ceramics with excitation at 450 nm. All the ceramics exhibited two apparent emission bands at 612 and 645 nm. These corresponded to the $^1D_2 \rightarrow {}^3H_4$ and $^3P_0 \rightarrow {}^3F_2$ transitions, respectively.[34]

A summary of the concentration-dependent emission intensity is shown in Figure 10c. It can be found with an increasing Pr^{3+} concentration, the intensity increased gradually and then reached a maximum at an x of 0.005. The further increase in the Pr^{3+} concentration led to a decrease in the PL density, which was related to the concentration quenching effect.[35,36] An *in situ* strong red emission could be seen in the BNBT-0.005Pr sample (shown in the inset of Figure 10b).
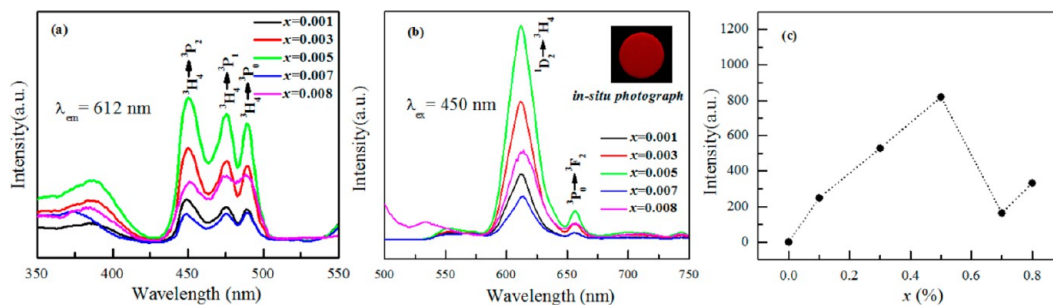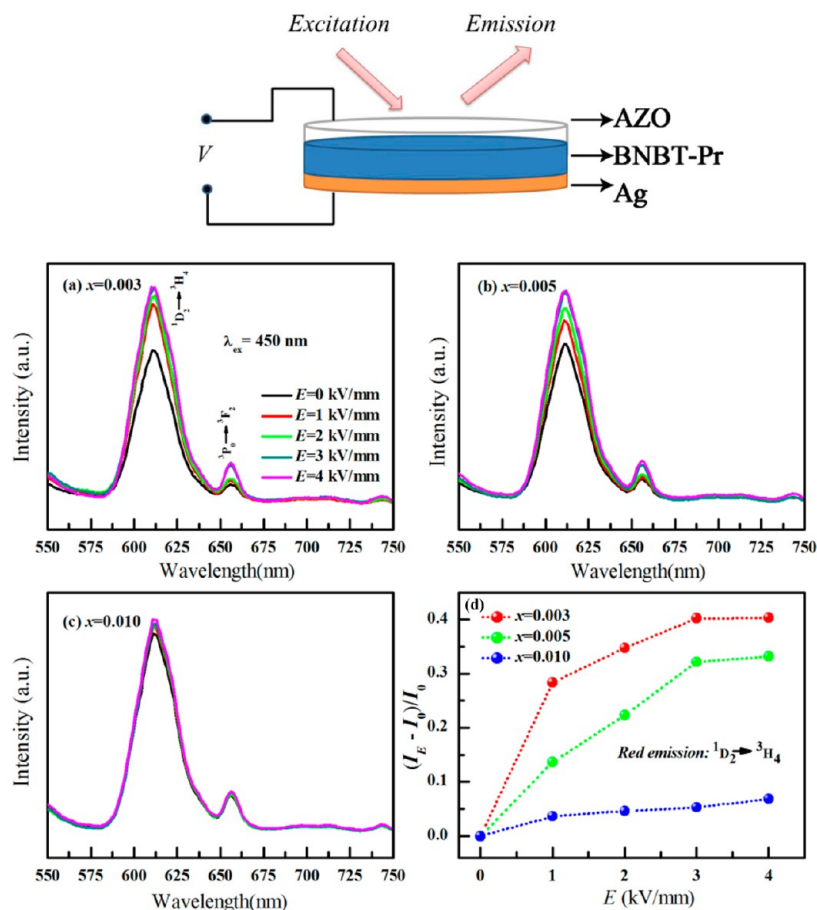

Figure 10. Composition-dependent (a) PL excitation and (b) emission spectra of the unpolarized BNBT-xPr with x values of 0.001, 0.003, 0.005, 0.007, and 0.008 and (c) a summary of the concentration-dependent emission intensity.

Figure 11. Schematic illustration of the experimental setup for measuring the *in situ* PL properties. (a−c) PL spectra for BNBT-0.003Pr, BNBT-0.005Pr, and BNBT-0.01Pr, respectively, under different *in situ* poling fields. (d) Composition and field dependence of the PL enhancement ratio $[(I_E − I_0)/I_0]$.

3.3. Strong Electric Field-Enhanced PL Effect and Ferroelectric/Photoluminescence Coupling Behavior.

It is well-known that enhancement of the PL is an important issue for widespread applications. How to realize the effective turning to enhance the PL intensity output has attracted a great deal of attention. Until now, modification of the PL intensity was generally realized by a chemical method as shown in the preceding section. This method is, however, generally irreversible, and the process is *ex situ*. Here, we propose an alternative way to realize the PL enhancement, and the PL intensity could be controlled through the ferroelectric polarization that had been reported in the ferroelectric thin film.[9] The field dependence of the PL intensity was systematically investigated, and a schematic illustration of the experimental setup is shown in Figure 11. An *in situ* poling field was applied to the sample during each PL test. It was noted that the sample was first coated with the electrode before the measurement, and transparent Al-doped ZnO (AZO) and Ag were chosen as the top and bottom electrode, respectively. The AZO transparent conductive electrode was deposited by a pulsed laser deposition method with a KrF excimer laser (wavelength of 248 nm) at 250 °C under an oxygen pressure of 0.1 Pa. Figure 11 shows the *in situ* electric field dependence of the PL intensity for BNBT-*x*Pr with *x* values of 0.003, 0.005, and 0.01 with excitation at 450 nm. As the poling field increased from 0 to 4 kV/mm, the PL intensity of BNBT-0.003Pr and BNBT-0.005Pr first increased to a maximum and then became saturated. A maximal PL enhancement of up to 40% was achieved in the BNBT-0.003Pr ceramic at 4 kV/mm. In

comparison, the field-induced PL enhancement of BNBT-0.01Pr was relatively weak (∼7%). The relationships among the composition, piezoelectric constant, and PL enhancement ratio $[(I_E − I_0)/I_0]$ are summarized in Figure 12.
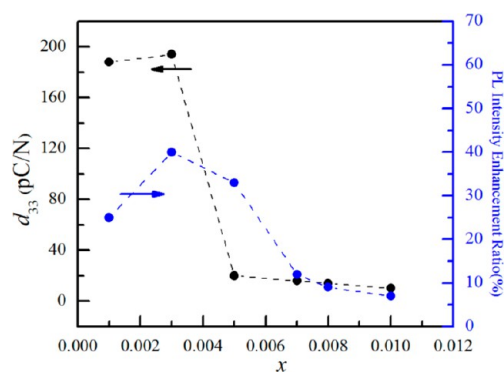
Figure 12. Composition-dependent d_{33} and the PL enhancement ratio $[(I_E − I_0)/I_0]$ at 4 kV/mm.

3.4. Discussion.

In this work, both the electric field-induced giant room-temperature strain response and enhanced PL were achieved in one solid solution, which provides a routine of ferroelectric control of the PL intensity and meanwhile opens up new piezoelectric and optical applications.

With regard to the structural reasons for the large strain response in BNT-based solid solutions, several mechanisms have
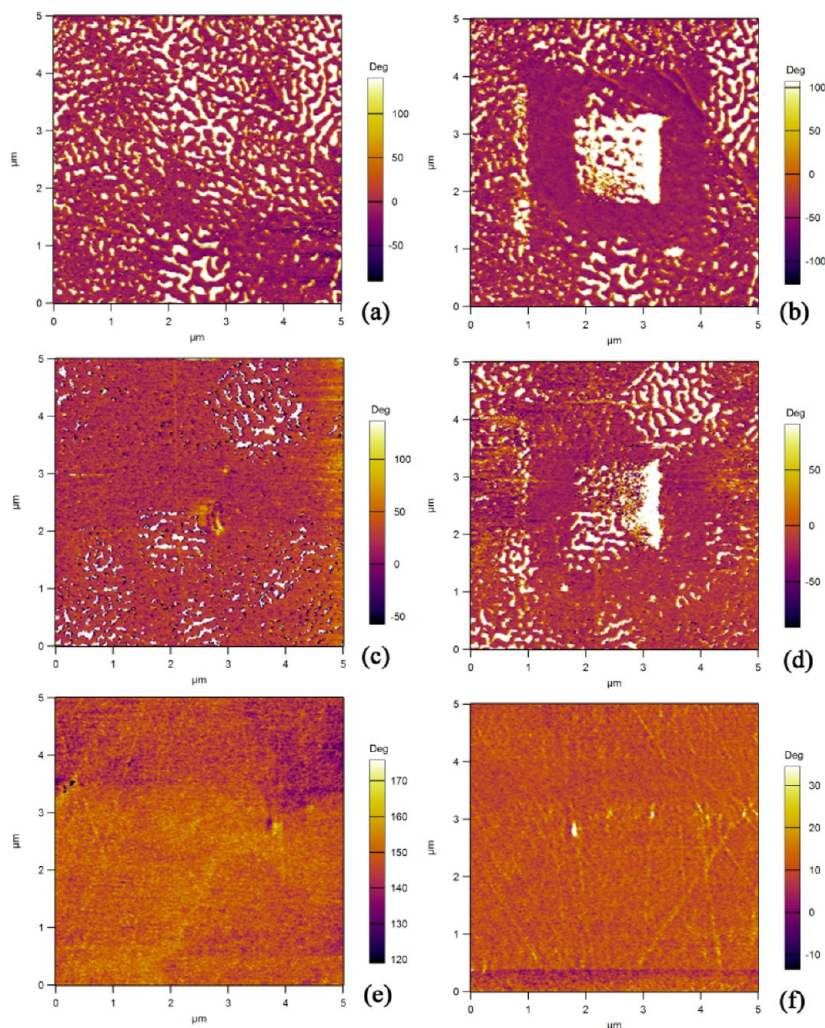
Figure 13. Piezoresponse phase image (5 μm × 5 μm) for BNBT, BNBT-0.008Pr, and BNBT-0.01Pr before (a, c, and e) and after poling (b, d, and f) under ∓5 V in 3 μm × 3 μm and 1 μm × 1 μm areas.

been proposed,[19,23,37−41] and previous discussions could also be found in our previous works.[23,41] In fact, the BNT-based system has quite complicated structures. Several phase diagrams have been proposed for binary $Bi_{0.5}Na_{0.5}TiO_3$-$BaTiO_3$ until now, and some issues are still unclear.[13,26,42−44] Recently, a monoclinic structure was even proposed in pure BNT.[45]

To clarify the field-induced phase transformation process, here the local poling experiments were further conducted by PFM, and the results are shown in Figure 13. For BNBT, from the out-of-plane piezoresponse image (poled under ∓5 V in 3 μm × 3 μm and 1 μm × 1 μm areas), clear contrast could be observed between the interior and the external square. This indicated the electric field-induced polarization rotation at microscale. A similar response was also observed for BNBT-0.003Pr. With the Pr concentration increasing to 0.008, only part of the domain could be observed at 5 V. This may be due to the domain relaxation and polarization switching after the field removal. With the concentration x further increasing to 0.10, little domain patterns could be observed. This should be ascribed to the weak ferroelectric polarization of BNBT-0.01Pr.

Using TEM,[39] X-ray neutron diffraction,[40] Raman,[44] and our XRD, Raman, PFM data, and electrical properties, we consider that the present BNBT-xPr with a large strain level (such as BNBT-0.008Pr) should be regarded as a relaxor ferroelectric state (macroscopically cubic while noncubic at nanoscale, which was verified by our PFM results) at ambient temperature. Even though some domain areas could be observed in the PFM image (Figure 3c,d), the dominant phase was a relaxor ferroelectric state. The reversible large strain response in BNBT-0.008Pr was caused by field-induced phase transformation from the ergodic relaxor pseudocubic state to the ferroelectric phase. After the field had been removed, the ergodic relaxor can bring it to the original status, and thus, a large reversible strain value could be obtained.

It is well-known that the 4f−4f electric dipole transition and PL intensity strongly depend on the internal crystal field and the host's symmetry.[9] Here to reveal the intrinsic mechanism for the field-induced enhancement in the PL property of BNBT-xPr, XRD patterns of both unpoled and poled samples were recorded (shown in Figure S4 of the Supporting Information). From the XRD patterns, the unpoled ceramics exhibited quite weak peak splitting. After they were poled at 4 kV/mm, the (111) and (200) peaks exhibited obvious peak splitting in BNBT-0.003Pr. This indicated that the external field could induce a phase transformation from the original pseudocubic phase to the coexistence of the rhombohedral and tetragonal phase. The corresponding d_{33} and k_t values of the poled BNBT-0.003Pr ceramic were 194 pC/N and 0.52, respectively. These results

indicate that polarization rotation and lattice distortion will be induced under an external field, leading to a lower crystal symmetry around the Pr^{3+} site. In principle, the lower symmetry can increase the electric dipole transition probabilities of the Pr^{3+} ions, which gives rise to the enhancement of PL emission. On the other hand, the ferroelectric polarization saturated gradually and the field amplitude of 4 kV/mm was enough to complete the phase transition for BNBT-0.003Pr and BNBT-0.005Pr. In comparison, a weak PL-enhancement effect (∼7%) was observed in the BNBT-0.01Pr ceramic because of the near nonferroelectric state, which was characterized by the small P_r of 7 $\mu C/cm^2$ and a d_{33} of ∼8 pC/N.

4. CONCLUSION

BNBT-xPr lead-free piezoelectric ceramics were fabricated through a traditional solid reaction method. The electrical and PL performances were systematically studied, and a schematic phase diagram was constructed. A giant strain with an S_{max}/E_{max} of up to 770 pm/V and an excellent PL-enhancement effect were achieved in this solid solution. We suggest that the giant strain response was attributed to the electric field-induced reversible phase transformation, while a PL enhancement of up to 40% was ascribed to the field-induced lattice distortion, together with the lower symmetry and different crystal fields. This multifunctional solid solution exhibited great potential in environmentally friendly "on−off" actuator and electric field-controlled PL devices.

■ ASSOCIATED CONTENT

Ⓢ Supporting Information

Temperature dependence of the electrical properties and some of the XRD data. This material is available free of charge via the Internet at http://pubs.acs.org.

■ AUTHOR INFORMATION

Corresponding Author

*Telephone and fax: +86-21-64328894. E-mail: f_f_w@sohu.com.

Notes

The authors declare no competing financial interest.

■ ACKNOWLEDGMENTS

■ REFERENCES

(1) Uchino, K. *Piezoelectric Actuators and Ultrasonic Motors*; Kluwer: Boston, 1997.

(2) Landau, L. D.; Lifshitz, E. M. *Electrodynamics of Continuous Media*; Pergamon: Oxford, U.K., 1960.

(3) Rack, P. D.; Holloway, P. H. The Structure, Device Physics, and Material Properties of Thin Film Electroluminescent Displays. *Mater. Sci. Eng., R* **1998**, *21*, 171−219.

(4) Grishina, A. M. Amplifying Magneto-Optical Photonic Crystal. *Appl. Phys. Lett.* **2010**, *97*, 061116.

(5) Mischenko, A. S.; Zhang, Q.; Scott, J. F.; Whatmore, R. W.; Mathur, N. D. Giant Electrocaloric Effect in Thin-Film $PbZr_{0.95}Ti_{0.05}O_3$. *Science* **2006**, *311*, 1270−1271.

(6) Wang, X. S.; Xu, C. N.; Yamada, H.; Nishikubo, H.; Zheng, X. G. Electro-Mechano-Optical Conversions in Pr^{3+}-Doped $BaTiO_3$-$CaTiO_3$ Ceramics. *Adv. Mater. (Weinheim, Ger.)* **2005**, *17*, 1254−1258.

(7) Rödel, J.; Jo, W.; Seifert, T. P. K.; Anton, E. M.; Granzow, T.; Damjanovic, D. Perspective on the Development of Lead-Free Piezoceramics. *J. Am. Ceram. Soc.* **2009**, *92*, 1153−1177.

(8) Liu, W. F.; Ren, X. B. Large Piezoelectric Effect in Pb-Free Ceramics. *Phys. Rev. Lett.* **2009**, *103*, 257602.

(9) Hao, J. H.; Zhang, Y.; Wei, X. H. Electric-Induced Enhancement and Modulation of Upconversion Photoluminescence in Epitaxial $BaTiO_3$:Yb/Er Thin Films. *Angew. Chem., Int. Ed.* **2011**, *50*, 6876−6880.

(10) Ganguly, P.; Joshi, T.; Singh, S.; Haranath, D.; Biradar, A. M. Electrically Modulated Photoluminescence in Ferroelectric Liquid Crystal. *Appl. Phys. Lett.* **2012**, *101*, 262902.

(11) Zhang, P. Z.; Shen, M. R.; Fang, L.; Zheng, F. G.; Wu, X. L.; Shen, J. C.; Chen, H. T. Pr^{3+} Photoluminescence in Ferroelectric $(Ba_{0.77}Ca_{0.23})TiO_3$ Ceramics: Sensitive to Polarization and Phase Transitions. *Appl. Phys. Lett.* **2008**, *92*, 222908.

(12) Zhou, H.; Chen, X. M.; Wu, G. H.; Gao, F.; Qin, N.; Bao, D. H. Significantly Enhanced Red Photoluminescence Properties of Nanocomposite Films Composed of a Ferroelectric $Bi_{3.6}Eu_{0.4}Ti_3O_{12}$ Matrix and Highly c-Axis-Oriented ZnO Nanorods on Si Substrates Prepared by a Hybrid Chemical Solution Method. *J. Am. Chem. Soc.* **2010**, *132*, 1790−1791.

(13) Takenaka, T.; Maruyama, K.; Sakata, K. $(Bi_{1/2}Na_{1/2})TiO_3$-$BaTiO_3$ System for Lead-Free Piezoelectric Ceramics. *Jpn. J. Appl. Phys.* **1991**, *30*, 2236−2239.

(14) Guo, Y. P.; Liu, Y.; Withers, R. L.; Brink, F.; Chen, H. Large Electric Field-Induced Strain and Antiferroelectric Behavior in (1-x)$(Na_{0.5}Bi_{0.5})TiO_3$-$x$$BaTiO_3$ Ceramics. *Chem. Mater.* **2011**, *23*, 219−228.

(15) Wang, F. F.; Xu, M.; Tang, Y. X.; Wang, T.; Shi, W. Z.; Leung, C. M. Large Strain Response in the Ternary $Bi_{0.5}Na_{0.5}TiO_3$-$BaTiO_3$-$SrTiO_3$ Solid Solutions. *J. Am. Ceram. Soc.* **2012**, *95*, 1955−1959.

(16) IEEE Standard on Piezoelectricity ANSI/IEEE 176, 1987.

(17) Shannon, R. D. Revised Effective Ionic Radii and Systematic Studies of Interatomic Distances in Halides and Chalcogenides. *Acta Crystallogr.* **1976**, *A32*, 751−767.

(18) Daniels, J. E.; Jo, W.; Rödel, J.; Jones, J. L. Electric-Field-Induced Phase Transformation at a Lead-Free Morphotropic Phase Boundary: Case Study in a 93%$(Bi_{0.5}Na_{0.5})TiO_3$-7%$BaTiO_3$ Piezoelectric Ceramic. *Appl. Phys. Lett.* **2009**, *95*, 032904.

(19) Zhang, S. T.; Kounga, A. B.; Aulbach, E.; Ehrenberg, H.; Rödel, J. Giant Strain in Lead-Free Piezoceramics $Bi_{0.5}Na_{0.5}TiO_3$-$BaTiO_3$-$K_{0.5}Na_{0.5}NbO_3$ System. *Appl. Phys. Lett.* **2007**, *91*, 112906.

(20) Hiruma, Y.; Nagata, H.; Takenaka, T. Detection of Morphotropic Phase Boundary of $(Bi_{1/2}Na_{1/2})TiO_3$-$Ba(Al_{1/2}Sb_{1/2})O_3$ Solid-Solution Ceramics. *Appl. Phys. Lett.* **2009**, *95*, 052903.

(21) Aksel, E.; Forrester, J. S.; Kowalski, B.; Deluca, M.; Damjanovic, D.; Jones, J. L. Structure and Properties of Fe-Modified $Na_{0.5}Bi_{0.5}TiO_3$ at Ambient and Elevated Temperature. *Phys. Rev. B* **2012**, *85*, 024121.

(22) Hao, J. G.; Bai, W. F.; Li, W.; Shen, B.; Zhai, J. W. Phase Transitions, Relaxor Behavior, and Large Strain Response in $LiNbO_3$-Modified $Bi_{0.5}(Na_{0.80}K_{0.20})_{0.5}TiO_3$ Lead-Free Piezoceramics. *J. Appl. Phys.* **2013**, *114*, 044103.

(23) Wang, F. F.; Leung, C. M.; Tang, Y. X.; Wang, T.; Shi, W. Z. Composition Induced Structure Evolution and Large Strain Response in Ternary $Bi_{0.5}Na_{0.5}TiO_3$-$Bi_{0.5}K_{0.5}TiO_3$-$SrTiO_3$ Solid Solution. *J. Appl. Phys.* **2013**, *114*, 164105.

(24) Smolenskii, G. A.; Isupov, V. A.; Agranovskaya, A. I.; Krainik, N. N. New Ferroelectrics of Complex Composition. IV. *Soviet Physics: Solid State* **1961**, *2*, 2651−2654.

(25) Anto, E. M.; Jo, W.; Damjanovic, D.; Rödel, J. Determination of Depolarization Temperature of $(Bi_{1/2}Na_{1/2})TiO_3$-Based Lead-Free Piezoceramics. *J. Appl. Phys.* **2011**, *110*, 094108.

(26) Jo, W.; Rödel, J. Electric-Field-Induced Volume Change and Room Temperature Phase Stability of $(Bi_{1/2}Na_{1/2})TiO_3$-x mol.% $BaTiO_3$ Piezoceramics. *Appl. Phys. Lett.* **2011**, *99*, 042901.

(27) Uchino, K.; Nomura, S. Critical Exponents of the Dielectric Constants in Diffused-Phase-Transition Crystals. *Ferroelectr., Lett. Sect.* **1982**, *44*, 55−61.

(28) Jo, W.; Dittmer, R.; Acosta, M.; Zang, J. D.; Groh, C.; Sapper, E.; Wang, K.; Rödel, J. Giant Electric-Field-Induced Strains in Lead-Free Ceramics for Actuator Applications: Status and Perspective. *J. Electroceram.* **2012**, *29*, 71−93.

(29) Jin, C. C.; Wang, F. F.; Wei, L. L.; Tang, J.; Li, Y.; Yao, Q. R.; Tian, C. Y.; Shi, W. Z. Influence of B-Site Complex-Ion Substitution on the Structure and Electrical Properties in $Bi_{0.5}Na_{0.5}TiO_3$-Based Lead-Free Solid Solutions. *J. Alloys Compd.* **2014**, *585*, 185−191.

(30) Sommerdijk, J. L.; Bril, A.; de Jager, A. W. Two Photon Luminescence with Ultraviolet Excitation of Trivalent Praseodymium. *J. Lumin.* **1974**, *8*, 341−343.

(31) Zhou, H.; Wu, G.; Gao, F.; Qin, N.; Bao, D. H. Improved Photoluminescence and Ferroelectric Properties of $(Bi_{3.6}Eu_{0.4})Ti_3O_{12}$ Thin Films via Li^+ Doping. *IEEE Transactions on Ultrasonics, Ferroelectrics, and Frequency Control* **2010**, *57*, 2134−2137.

(32) Chi, L.; Liu, R.; Lee, B. Synthesis of Y_2O_3:Eu, Bi Red Phosphors by Homogeneous Coprecipitation and Their Photoluminescence Behaviors. *J. Electrochem. Soc.* **2005**, *152*, J93−J98.

(33) Sun, H. Q.; Peng, D. F.; Wang, X. S.; Tang, M. M.; Zhang, Q. W.; Yao, X. Strong Red Emission in Pr Doped $(Bi_{0.5}Na_{0.5})TiO_3$ Ferroelectric Ceramics. *J. Appl. Phys.* **2011**, *110*, 016102.

(34) Haranath, D.; Khan, A. F.; Chander, H. Bright Red Luminescence and Energy Transfer of Pr^{3+}-Doped $(Ca, Zn)TiO_3$ Phosphor for Long Decay Applications. *J. Phys. D: Appl. Phys.* **2006**, *39*, 4956−4960.

(35) Chawla, S.; Kumar, N.; Chander, H. Broad Yellow Orange Emission from $SrAl_2O_4$:Pr^{3+} Phosphor with Blue Excitation for Application to White LEDs. *J. Lumin.* **2009**, *129*, 114−118.

(36) Rai, V. K.; Rai, S. B.; Rai, D. K. Spectroscopic Properties of Pr^{3+} Doped in Tellurite Glass. *Spectrochim. Acta, Part A* **2005**, *62*, 302−306.

(37) Jo, W.; Granzow, T.; Aulbach, E.; Rodel, J.; Damjanovic, D. Origin of the Large Strain Response in $(K_{0.5}Na_{0.5})NbO_3$-Modified $Bi_{0.5}Na_{0.5}TiO_3$-$BaTiO_3$ Lead-Free Piezoceramics. *J. Appl. Phys.* **2009**, *105*, 094102.

(38) Hussain, A.; Ahn, C. W.; Lee, J. S.; Ullah, A.; Kim, I. W. Large Electric-Field-Induced Strain in Zr-Modified Lead-Free $Bi_{0.5}(Na_{0.78}K_{0.22})_{0.5}TiO_3$ Piezoelectric Ceramics. *Sens. Actuators, A* **2010**, *158*, 84−89.

(39) Kling, J.; Tan, X.; Jo, W.; Kleebe, H.-J.; Fuess, H.; Rödel, J. In Situ Transmission Electron Microscopy of Electric Field-Triggered Reversible Domain Formation in Bi-Based Lead-Free Piezoceramics. *J. Am. Ceram. Soc.* **2010**, *93*, 2452−2455.

(40) Hinterstein, M.; Knapp, M.; Hölzel, M.; Jo, W.; Cervellino, A.; Ehrenberg, H.; Fuess, H. Field-Induced Phase Transition in $Bi_{1/2}Na_{1/2}TiO_3$-Based Lead-Free Piezoelectric Ceramics. *J. Appl. Crystallogr.* **2010**, *43*, 1314−1321.

(41) Li, Y.; Wang, F. F.; Ye, X.; Xie, Y. Q.; Tang, Y. X.; Sun, D. Z.; Shi, W. Z.; Zhao, X. Y.; Luo, H. S. Large Strain Response and Fatigue-Resistant Behavior in Ternary $Bi_{0.5}Na_{0.5}TiO_3$-$BaTiO_3$-$Bi(Zn_{0.5}Ti_{0.5})O_3$ Solid Solutions. *J. Am. Ceram. Soc.* **2014**, *97*, 3615−3623.

(42) Hiruma, Y.; Watanabe, Y.; Nagata, H.; Takenaka, T. Phase Transition Temperatures of Divalent and Trivalent Ions Substituted $(Bi_{1/2}Na_{1/2})TiO_3$ Ceramics. *Key Eng. Mater.* **2007**, *350*, 93−96.

(43) Ma, C.; Tan, X.; Dul'kin, E.; Roth, M. Domain Structure-Dielectric Property Relationship in Lead-Free $(1−x)(Bi_{1/2}Na_{1/2})TiO_3$-$xBaTiO_3$ Ceramics. *J. Appl. Phys.* **2010**, *108*, 104105.

(44) Wylie-Van Eerd, B.; Damjanovic, D.; Klein, N.; Setter, N.; Trodahl, J. Structural Complexity of $(Na_{0.5}Bi_{0.5})TiO_3$-$BaTiO_3$ as Revealed by Raman Spectroscopy. *Phys. Rev. B* **2010**, *82*, 104112.

(45) Aksel, E.; Forrester, J. S.; Jones, J. L.; Thomas, P. A.; Page, K.; Suchomel, M. R. Monoclinic Crystal Structure of Polycrystalline $Na_{0.5}Bi_{0.5}TiO_3$. *Appl. Phys. Lett.* **2011**, *98*, 152901.